





The classification and formation rate of Swift/BAT gamma-ray bursts*

JUAN-JUAN LUO ¹, LIANG ZHANG ², LI-YUN ZHANG ³, YONG-FENG HUANG ^{4,5}, JIA-QUAN LIN,² JUN-WANG LU,¹
AND XIAO-FEI DONG⁴

¹*School of Physics and Electronics, Qiannan Normal University for Nationalities, Duyun 558000, P. R. China*[†]

²*Guizhou Vocational College of Economics and Business, Duyun 558022, P. R. China*[‡]

³*College of Science, Guizhou University and NAOC-GZU-Sponsored Center for Astronomy, Guizhou University, Guiyang 550025, P. R. China*[§]

⁴*School of Astronomy and Space Science, Nanjing University, Nanjing 210023, P. R. China*[¶]

⁵*Key Laboratory of Modern Astronomy and Astrophysics (Nanjing University), Ministry of Education, P. R. China*

(Received ?; Revised ?; Accepted ?)

Submitted to ApJL

ABSTRACT

Gamma-ray bursts (GRBs) are usually classified into long/short categories according to their durations, but controversy still exists in this aspect. Here we re-examine the long/short classification of GRBs and further compare the cosmological distribution and evolution of each potential subclass. A large number of *Swift/BAT* GRBs are analyzed in this study. The Gaussian mixture model is used to fit the duration distribution as well as the joint distribution of duration and hardness ratio, and the Akaike and Bayesian information criteria are adopted to assess the goodness of fit. It is found that three Gaussian components can better fit both the univariate and bivariate distributions, indicating that there are three subclasses in the *Swift/BAT* GRBs, namely short, intermediate, and long subclasses. The non-parametric Efron-Petrosian and Lynden-Bell's c^- methods are used to derive the luminosity function and formation rate from the truncated data of bursts with known redshift in each subclass. It is found that the luminosity distributions and birth rates of the three subclasses are different, further supporting the existence of the intermediate subclass in the *Swift/BAT* GRBs.

Keywords: gamma-ray bursts: classification – stars: formation rate– stars: luminosity function – methods: statistical

1. INTRODUCTION

Thousands of Gamma-ray bursts (GRBs, Klebesadel et al. (1973)) have been detected from the sky up to now. Based on their durations (T_{90} , Kouveliotou et al. (1993)), GRBs can be generally be classified into two groups, i.e. short GRBs (sGRBs) and long GRBs (lGRBs). Short GRBs are believed to originate from mergers of double neutron stars (NS-NS) or NS-black hole binaries, while lGRBs are thought to come from the collapse of massive stars at the end of their lives (Woosley 1993; Paczyński 1998; Woosley & Bloom 2006; Zhang et al. 2022). In this framework, the event rate of lGRBs should naturally trace the star formation rate (SFR) (Butler et al. 2010; Elliott et al. 2012; Wang 2013).

The idea of classifying GRBs according to their T_{90} can be traced back to the *CGRO/BATSE* era. It was found that the distribution of T_{90} can be well fitted by two lognormal components (Kouveliotou et al. 1993; McBreen et al. 1994), which correspond to sGRBs group and lGRBs group. Interestingly, Horváth (1998) noticed that there is an intermediate group located between short and long groups. However, as the number of GRBs in the *CGRO/BATSE*

* Released on May, 3st, 2024

† E-mail: j-j_luo@sina.com

‡ E-mail: liang_zhang_gz@sina.com

§ E-mail: liy_zhang@hotmail.com

¶ E-mail: hyf@nju.edu.cn

catalogue increases, the existence of the intermediate component seems to be less apparent (Horváth 2002; Tarnopolski 2015; Zhang et al. 2022). Since then, such a third component has been widely paid attention to and controversial results are obtained. For example, Zitouni et al. (2015) analyzed 248 *Swift*/*BAT* GRBs with known redshift, claiming that the intermediate group is present rather clearly in the fitting of T_{90} in both the observer and rest frame. Tarnopolski (2015) analyzed ~ 1500 *Fermi*/*GBM* GRBs and also concluded that the T_{90} distribution is well fitted by a mixture of three log-normal distributions, indicating the presence of the intermediate class. On the other hand, Zhang et al. (2016) composed large samples consisting of 2037 *CGRO*/*BATSE* GRBs, 956 *Swift*/*BAT* GRBs (298 events with redshift available), and 1741 *Fermi*/*GBM* GRBs, respectively. They found that the two-Gaussian (2-G) model is strongly supported by *CGRO*/*BATSE* and *Fermi*/*GBM* samples, while the *Swift*/*BAT* sample supports the three-Gaussian (3-G) model. Additionally, the number of GRBs in the sample has a significant impact on the classification of GRBs. Zhang et al. (2022) have conducted a detailed study on the impact of sample size on the classification of GRBs and found that the intermediate group could be concealed when the sample size is large. Theoretically, an important reason that leads to the doubtful existence of intermediate group is the lack of progenitor stars that could produce these special events.

The *Swift*/*BAT* catalogue includes many GRBs with redshift available (Gehrels et al. 2004), which makes it possible to study the event rate of IGRBs. Based on these events, researchers have investigated possible evolution of the luminosity function with respect to redshift as well as the relationship between GRB event rate and the SFR (Liang et al. 2007; Wanderman & Piran 2010; Cao et al. 2011; Salvaterra et al. 2012; Robertson & Ellis 2012; Howell et al. 2014; Petrosian et al. 2015; Yu et al. 2015; Deng et al. 2016; Pescalli et al. 2016; Zhang & Wang 2018; Dainotti et al. 2021b; Dong et al. 2022; Petrosian & Dainotti 2024). Therefore, studying the cosmological distribution and evolution of each subclass of GRBs can provide useful information on their physical origins.

In this study, we collect a large *Swift*/*BAT* GRB sample, based on which the univariate duration (T_{90}) distribution and bivariate T_{90} versus hardness ratio (HR) distribution are analyzed. Various subclasses are identified and their redshift distribution and cosmological evolution are compared. The structure of our paper is organized as follows. A detailed description of the data acquisition and the sample constitution is presented in Section 2. The methods adopted to analyze the samples are described in Section 3. Here, we use the Gaussian Mixture Model (GMM) to assess the T_{90} distribution and use both the Akaike information criteria (AIC) and Bayesian information criteria (BIC) to evaluate the fitting results comprehensively. Due to the unavoidable observational selection effect of the *Swift*/*BAT* detector, the sample is a truncated and incomplete collection. We use the non-parametric Efron-Petrosian (EP) method (Efron & Petrosian 1992) to eliminate the redshift evolution of the luminosity, and use the Lynden-Bell's c^- method (Lynden-Bell 1971) to derive the intrinsic luminosity function and event rate of GRBs. Our numerical results are presented in Section 4. Finally, Section 5 presents our conclusions and discussion. Throughout this study, we assume a flat Λ CDM cosmology with $\Omega_m = 0.27$ and $H_0 = 70 \text{ km s}^{-1} \text{ Mpc}^{-1}$.

2. DATA SELECTION

As of February 18, 2024, the *Swift*/*BAT* GRB Catalog ¹ contains 1832 GRBs, of which 440 events have redshift measurements. In order to study the long/short classification of GRBs, we have grouped the bursts into two samples: Sample I contains all the 1512 *Swift*/*BAT* GRBs with valid T_{90} data; Sample II contains 1454 *Swift*/*BAT* GRBs with both valid T_{90} and spectral hardness ratio data. The hardness ratio is usually defined as

$$HR = \frac{S_{50-100\text{keV}}}{S_{15-25\text{keV}}} = \frac{\int_{50\text{keV}}^{100\text{keV}} F(E)E dE}{\int_{15\text{keV}}^{25\text{keV}} F(E)E dE}, \quad (1)$$

where $F(E)$ is the spectrum which could generally be fit by a power-law or cut-off power-law function.

In order to study the cosmological distribution and evolution of each subclass, the peak luminosity (L_p) of each GRB should be known, which further requires that several other parameters should be available. They include the redshift, the spectral index, as well as the peak flux in the energy range of 15 — 150 keV. In our study, L_p is calculated by using $L_p = 4\pi d_L^2(z)FK(z)$, where $d_L(z)$ denotes the luminosity distance, $K(z)$ denotes the K-correction, F denotes the peak flux in units of photons $\text{cm}^{-2} \text{ s}^{-1}$ in the energy range of 15 keV — 150 keV for *Swift*/*BAT*. Dainotti et al. (2021b) pointed out that the luminosity evolution (i.e., the dependence of luminosity on the redshift) is sensitive to

¹ https://swift.gsfc.nasa.gov/archive/grb_table/

the flux limit. An improper selection of the flux limit could lead to a false luminosity evolution. In our study, we adopt two flux limits, $F_{\text{limit},1} = 2.0 \times 10^{-8}$ erg cm $^{-2}$ s $^{-1}$ and $F_{\text{limit},2} = 5.0 \times 10^{-9}$ erg cm $^{-2}$ s $^{-1}$, to overcome this problem as far as possible. $F_{\text{limit},1}$ is used for short GRBs; while $F_{\text{limit},2}$ is used for intermediate GRBs and long events. The limiting luminosity is then expressed as $L_{\text{limit}} = 4\pi d_L^2(z) F_{\text{limit}} \bar{K}(z)$ (Petrosian et al. 2015), where the K-correction term $\bar{K}(z)$ is calculated by assuming a simple power law spectrum with a mean spectral index of -1.1 (Zhang et al. 2018).

3. METHODS

Fitting the T_{90} distribution with multiple Gaussian components is widely adopted in the long/short classification of GRBs. The focus is how to optimize the objective function to determine the appropriate number of Gaussian components and obtain the parameters for each component. For example, Horváth (1998, 2002); Tarnopolski (2015); Zitouni et al. (2015) used χ^2 fitting to analyze the T_{90} distribution. Tsutsui & Shigeyama (2014); Zhang et al. (2016, 2022) used the Gaussian mixture model (GMM) algorithm to study the long/short classification of GRBs. Since the χ^2 fitting is affected by input data binning strategy, here we adopt the GMM algorithm in our study. The probability density function (PDF) of K components GMM is

$$p(\mathbf{x}) = \sum_{k=1}^K A_k \mathcal{N}(\mathbf{x}; \boldsymbol{\mu}_k, \boldsymbol{\Sigma}_k), \quad (2)$$

where $\mathcal{N}(\mathbf{x}; \boldsymbol{\mu}_k, \boldsymbol{\Sigma}_k)$ represents the PDF of each component, \mathbf{x} represents a M -dimensional data vector: $\mathbf{x} = x_j (j = 1, 2, \dots, M)$ (Tsutsui & Shigeyama 2014). The weights satisfy $\sum_{k=1}^K A_k = 1$. For the k th Gaussian component, the PDF is

$$\mathcal{N}(\mathbf{x}; \boldsymbol{\mu}_k, \boldsymbol{\Sigma}_k) = \frac{1}{2\pi \sqrt{|\boldsymbol{\Sigma}_k|}} \exp \left[-\frac{1}{2} (\mathbf{x} - \boldsymbol{\mu}_k)^T \boldsymbol{\Sigma}_k^{-1} (\mathbf{x} - \boldsymbol{\mu}_k) \right], \quad (3)$$

where $\boldsymbol{\mu}_i$ is the mean value and $\boldsymbol{\Sigma}_i$ is the covariance matrix, with $|\boldsymbol{\Sigma}_i| = \det(\boldsymbol{\Sigma}_i)$.

Tsutsui & Shigeyama (2014) pointed out that given a sequence of independent data $\mathbf{X} = \{\mathbf{x}_1, \mathbf{x}_2, \dots, \mathbf{x}_N\}$, the logarithmic likelihood function is

$$\ln p(\mathbf{X}; \mathbf{A}, \boldsymbol{\mu}, \boldsymbol{\Sigma}) = \sum_{i=1}^N \ln \left[\sum_{k=1}^K A_k \mathcal{N}(\mathbf{x}_i; \boldsymbol{\mu}_k, \boldsymbol{\Sigma}_k) \right]. \quad (4)$$

The goal is to maximize the likelihood function to determine the optimal parameters of the model. By taking partial derivatives of the log likelihood function with respect to $\boldsymbol{\mu}_k$ and $\boldsymbol{\Sigma}_k$ and letting them equal to zero, expressions of the above parameters can be obtained as

$$\boldsymbol{\mu}_k = \frac{1}{N_k} \sum_{i=1}^N \gamma_{ik} \mathbf{x}_i, \quad (5)$$

$$\boldsymbol{\Sigma}_k = \frac{1}{N_k} \sum_{i=1}^N \gamma_{ik} (\mathbf{x}_i - \boldsymbol{\mu}_k) (\mathbf{x}_i - \boldsymbol{\mu}_k)^T, \quad (6)$$

where

$$N_k = \sum_{i=1}^N \gamma_{ik}, \quad (7)$$

and γ_{ik} is called the responsibility, which represents the probability that a particular event belongs to each cluster. It can be calculated as

$$\gamma_{ik} = \frac{A_k \mathcal{N}(\mathbf{x}_i; \boldsymbol{\mu}_k, \boldsymbol{\Sigma}_k)}{\sum_{j=1}^K A_j \mathcal{N}(\mathbf{x}_i; \boldsymbol{\mu}_j, \boldsymbol{\Sigma}_j)}. \quad (8)$$

The proportion coefficient A_k of each Gaussian component is determined by

$$A_k = \frac{N_k}{N}, \quad (9)$$

which is derived using the Lagrange multiplier method.

Table 1. The ranges and corresponding descriptions of ΔAIC_i and ΔBIC_i

name	range	description ^a
ΔAIC_i	(0,2)	a substantial support for the i th model
	(2,4)	a strong support for the i th model
	(4,7)	a considerably less support for the i th model
	>7	essentially no support for the i th model
ΔBIC_i	(0,2)	a substantial support for the i th model
	(2,6)	an evidence against the i th model
	(6,10)	a strong evidence against the i th model
	>10	a very strong evidence against the i th model

Note. ^aReferences: Kass & Raftery (1995); Burnham & Anderson (2004); Tarnopolski (2019); Zhang et al. (2022)

From Equations 5, 6 and 9, it can be seen that the key to derive the model parameters is to determine γ_{ik} . However, γ_{ik} itself is a function of model parameters. Therefore, the expectation-maximization algorithm is introduced in our study, which is an iterative process used to solve the optimal parameters of probability models containing latent variables (Tsutsui & Shigeyama 2014). The steps are as following: (i) Initialize the model parameters of A_k , $\boldsymbol{\mu}_k$, $\boldsymbol{\Sigma}_k$, and calculate the value of the logarithmic likelihood; (ii) Calculate the γ_{ik} values using Equation 8; (iii) Recalculate the values of the model parameters using γ_{ik} obtained in Step ii; (iv) Repeat Step (ii) and Step (iii) until the likelihood function converge. In this way, the optimal model parameters can be self-consistently determined. Note that the GMM and EM algorithm has been implemented in the **PYTHON** machine learning package of **sklearn.mixture**², which is used in our study.

The Akaike information criterion (AIC, Akaike (1974)) and Bayesian information criterion (BIC, Schwarz (1978)) are widely used in assessing the goodness of models in astronomy (Liddle 2007). They are defined as $AIC = 2p - 2 \ln P_{\max}$ and $BIC = p \ln N - 2 \ln P_{\max}$, respectively, where p represents the number of parameters of the model, N represents the sample size, and P_{\max} represents the maximum value of the likelihood function. It is worth noting that when $N > 8$, the first term of AIC and BIC satisfies $p \ln N > 2p$, indicating that the penalty term of BIC is much larger than that of AIC, especially for a large sample size. Furthermore, a larger penalty term in BIC may lead to underfitting (resulting in a simple model with fewer parameters), while a smaller penalty term in AIC may lead to overfitting (resulting in a complex model with more parameters). These criteria for model selection have been widely applied in previous studies on GRB classification (Tsutsui & Shigeyama 2014; Zhang et al. 2016; Tarnopolski 2019; Zhang et al. 2022). Therefore, for the current GRB long/short classification problem, we adopt the AIC and BIC criteria to determine the best fitting model for each sample, which can achieve a good balance between the two competing terms so that it generally has the minimum AIC and BIC values (hereafter AIC_{\min} , BIC_{\min}). For the i th model, the AIC difference is calculated as $\Delta AIC_i = AIC_i - AIC_{\min}$, and the BIC difference is $\Delta BIC_i = BIC_i - BIC_{\min}$. The range of ΔAIC_i and ΔBIC_i and the corresponding descriptions are detailedly shown in Table 1.

Previous studies indicate that the luminosity (L) and redshift (z) of GRBs are not independent. Determination of the cosmological GRB distribution requires that the $L - z$ relation should be established first. Efron & Petrosian (1992) developed a useful method that is very effective in this aspect. It can be applied to both one sided truncation (Efron & Petrosian 1992) and two sided truncation samples (Efron & Petrosian 1998). The Efron-Petrosian (EP) method has been adopted to determine the luminosity evolution in many astronomical fields (Yonetoku et al. 2004; Yu et al. 2015; Tsvetkova et al. 2017; Zhang & Wang 2018; Dong et al. 2022). In this study, we also use the EP method to derive the luminosity evolution of GRBs, which is characterized by a redshift-dependent term of $g(z)$. The de-evolved luminosity in the GRB local frame can then be calculated as $L_0 = L/g(z)$. As usual, we assume that $g(z)$ takes the form of a power-law function, $g(z) = (1 + z)^k$. Details on determining the index k through the EP method can be found in Efron & Petrosian (1992).

After deriving the de-evolved luminosity L_0 , the local cumulative luminosity function $\psi(L_0)$ and the cumulative redshift distribution $\phi(z)$ can be derived by using the Lynden-Bell's c^- method (Lynden-Bell 1971). This method was rediscovered for its wide application in recovering truncated luminosity functions by (Woodroffe 1985) and Wang et al. (1986), and is extensively discussed in Efstathiou et al. (1988); Efron & Petrosian (1992); Dörre & Emura (2019). It is a unique nonparametric procedure applicable to randomly truncated univariate data, which has already been interestingly used in the field of GRBs (e.g. Dainotti et al. (2013, 2015, 2017a,b, 2020, 2021b,a, 2022); Lloyd &

² <https://scikit-learn.org/stable/modules/mixture.html#gaussian-mixture>

Table 2. The results of AIC and BIC values for Samples I and II. For the distribution of GRBs in each sample, a mixture of 1 to 6 Gaussian components are tested.

No. ^a	Sample I ^c		Sample II ^c	
	AIC	BIC	AIC	BIC
min ^b	3265.21	3307.78	2675.07	2764.87
1	333.65	301.72	506.45	443.07
2	30.88	14.92	75.45	43.76
3	0	0	0	0
4	12.18	28.15	1.38	33.07
5	16.50	48.43	90.3	72.41
6	17.19	65.08	15.52	110.60

Note. ^aThe number of Gaussian component. ^bThe “min” row lists the minimum AIC and BIC values obtained for each sample with GMM of 1 to 6 components, which correspond to the best fit model. The data marked in boldface in this row are true AIC and BIC values. The data in other rows are differential values of ΔAIC and ΔBIC with respect to the “min” row. ^cThe number of GRBs in Samples I and II is 1512, 1401, respectively.

Petrosian (1999); Yonetoku et al. (2004); Yu et al. (2015); Tsvetkova et al. (2017); Zhang & Wang (2018); Dong et al. (2022)). It is worth noting that our samples are also truncated data since the energy range and sensitivity (the flux threshold) of *Swift/BAT* are always limited during the observations. Considering these unavoidable observational selection effects, we will use the non-parametric Efron-Petrosian and Lynden-Bell’s c^- method (EP-L, for short) to study the cosmological distribution and evolution of different subclasses of GRBs. For details on determining the local cumulative luminosity function $\psi(L_0)$ and the cumulative redshift distribution $\phi(z)$ of *Swift/BAT* GRBs through the EP-L method, please refer to Petrosian et al. (2015); Yu et al. (2015); Dong et al. (2022).

4. RESULTS

4.1. Long/short classification of GRBs

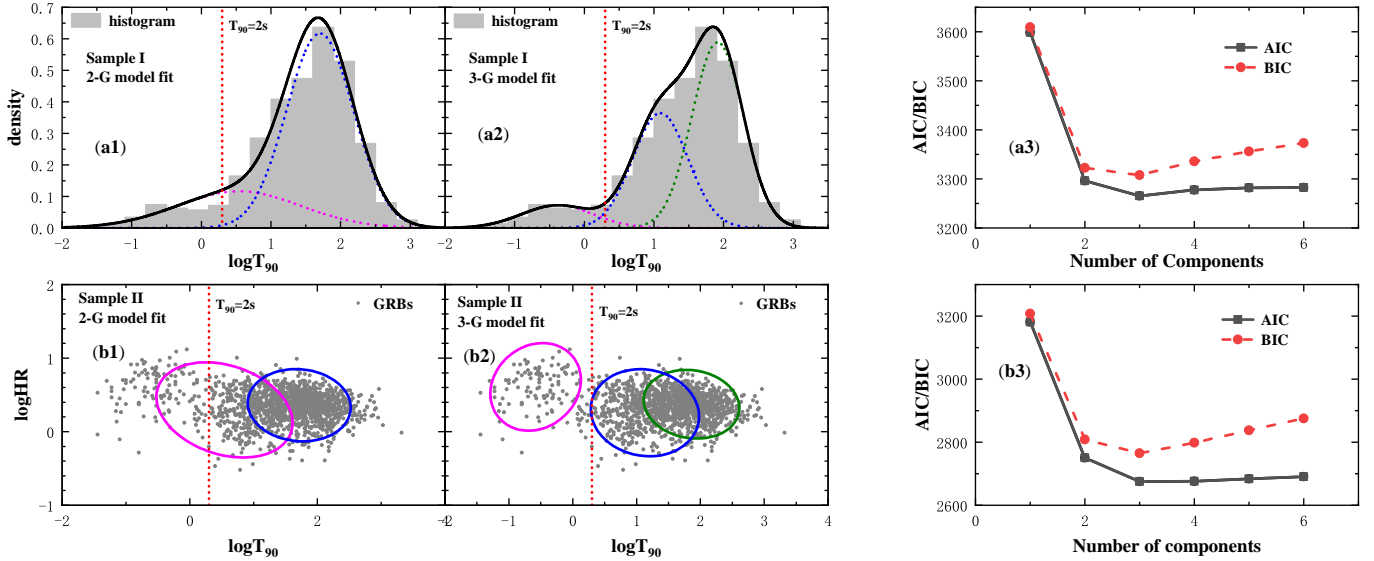


Figure 1. Fitting Samples I and II by using the GMM models. The upper panels show the T_{90} distribution of Sample I fitted with the 2-G and 3-G models, together with the AIC/BIC values. In (a1) and (a2) panels, the solid curves show the superposed total PDF of the 2-G model and 3-G model, while the dashed curves show the contribution of different components. The lower panels illustrate the joint distribution of T_{90} – HR for Sample II, fitted with the 2-G and 3-G models. Both the X- and Y-axis are in logarithmic coordinates. The (b1) panel shows the full width of half maximum (FWHM) of each component in the framework of the 2-G model, and the (b2) panel correspondingly shows the 3-G model fitting results. The dotted vertical lines represent $T_{90} = 2$ s. In (a3) and (b3) panels, it could be seen that both AIC and BIC criteria support the 3-G model for Samples I and II.

We have used the one-dimensional GMM model to fit the T_{90} distribution of Sample I. A two-dimensional GMM model is also applied on Sample II to consider the joint effects of T_{90} and HR on the classification. The AIC and BIC values obtained in the fitting are presented in Table 2. Figure 1 illustrates the fitting results of the 2-G model and 3-G model to these two samples.

From the second and third columns of Table 2, it can be seen that the 3-component model gives the best description for the T_{90} distribution of Sample I, which is consistent with previous studies (Horváth 2002; Tarnopolski 2015, 2019; Zhang et al. 2016). The minimum values of AIC and BIC are correspondingly $AIC_3 = 3265.21$ and $BIC_3 = 3307.78$. Additionally, as a comparison, we have $\Delta AIC_2 = 30.88$ and $\Delta BIC_2 = 14.92$ for the two component model. Zhang et al. (2016) have conducted a similar study using two *Swift/BAT* samples (with 708 and 956 GRBs respectively). They concluded that the 3-G model was the best fitting model. In their work, ΔBIC_2 is approximately 5.5 for the two component model. Considering that the number of GRBs in our Sample I is more than twice of that of Zhang et al. (2016), a larger ΔBIC_2 obtained by us thus can be regarded as a strong support for the existence of the intermediate subclass. In the upper panels of Figure 1, we could also see that the 3-G model generally presents a better fit to the observations than the 2-G model. Panel (a3) shows that both AIC and BIC tests support the 3-G model for Sample I.

Similarly, the fourth and fifth columns of Table 2 show that the 3-component model also gives the best description for the $T_{90} - \text{HR}$ distribution of Sample II. The minimum values of AIC and BIC are correspondingly $AIC_3 = 2675.07$ and $BIC_3 = 2764.87$, which is consistent with the above conclusion drawn by only considering the T_{90} parameter. In the lower panels of Figure 1, there are two contour curves in the (b1) panel and three contour curves in the (b2) panel. The pink contour mainly includes sGRBs while the green contour contains most of the LGRBs. The blue contour in the (b2) panel corresponds to the intermediate component, which are also relatively long GRBs. We could see that the 3-G model generally presents a better fit to the observations than the 2-G model. Especially, we notice that for the 2-G model, we have $\Delta AIC_2 = 75.45$ and $\Delta BIC_2 = 43.76$ in Sample II, which are correspondingly larger than that in Sample I ($\Delta AIC_2 = 30.88$ and $\Delta BIC_2 = 14.92$). So, the support for the 3-G model is further strengthened in Sample II as compared with Sample I. In short, the inclusion of the HR parameter further strengthens the existence of the intermediate subclass of GRBs.

4.2. Luminosity function and event rate

According to the above analysis, GRBs should be classified into three groups, the short group (SGRBs), intermediate group (MGRBs), and long group (LGRBs). Here we go further to study the cosmological distribution and evolution of these three groups using the EP-L method. For this purpose, an additional parameter of redshift (z) is required to calculate the peak luminosity L_p of each GRB (see Section 2). Ultimately, for SGRBs, there are only 25 GRBs meeting this requirement. Similarly, for MGRBs and LGRBs, the numbers of available events are 126 and 255, respectively. In our analysis below, the flux limit $F_{\text{limit},1}$ is adopted for SGRBs, while $F_{\text{limit},2}$ is adopted for MGRBs and LGRBs.

As the first step, we use the non-parametric Efron-Petrosian (EP) method to determine the luminosity evolution of each group. As described in Section 3, the luminosity evolution is assumed to take the form of $g(z) = (1+z)^k$. The panels of (a1), (a2), and (a3) in Figure 2 illustrate the test statistic τ versus k for the three subclasses of GRBs. For SGRBs, the k index is derived as $k = 4.43_{-1.06}^{+1.03}$ at 1σ confidence level. For MGRBs and LGRBs, the indices are $k = 2.86_{-0.55}^{+0.43}$ and $k = 2.56_{-0.27}^{+0.33}$, respectively. Obviously, the k parameter is different for the three groups. Our k value of SGRBs is consistent with previous works that studied the luminosity evolution of short GRBs (Zhang & Wang 2018; Dainotti et al. 2021b), and our k value of LGRBs is also consistent with previous results concerning long GRBs (Yonetoku et al. 2004; Yu et al. 2015; Petrosian et al. 2015; Pescalli et al. 2016). Using the k parameter, the de-evolved luminosity can be calculated as $L_0 = L/(1+z)^{4.43}$, $L_0 = L/(1+z)^{2.86}$, and $L_0 = L/(1+z)^{2.56}$ for SGRBs, MGRBs and LGRBs, respectively. The de-evolved luminosity L_0 versus redshift z of the three samples are illustrated in the panels of (b1), (b2), and (b3) of Figure 2.

Then, we can use the Lynden-Bell's c^- method to derive the non-evolving cumulative luminosity function $\psi(L_0)$ and the cumulative redshift distribution $\phi(z)$ of SGRBs, MGRBs, and LGRBs. The results are shown in Panels (c) and (d) of Figure 2, respectively. From Panel (c), it can be seen that the profiles of $\psi(L_0)$ are different from for the three groups. Especially, the $\psi(L_0)$ of MGRBs is lower than those of LGRBs and SGRBs, indicating that MGRBs are mainly low luminosity bursts. The Kolmogorov-Smirnov (K-S) test has been adopted to compare the cumulative luminosity function of each pair of the three groups, which gives the P-values as $p_{12} = 7.9 \times 10^{-3}$, $p_{13} = 4.3 \times 10^{-2}$, and $p_{23} = 0.21$. Again, it strongly indicates that the intermediate class does exist, rather than being a vassal of the long class. A broken power-law function has been adopted to fit the normalized cumulative luminosity function. For

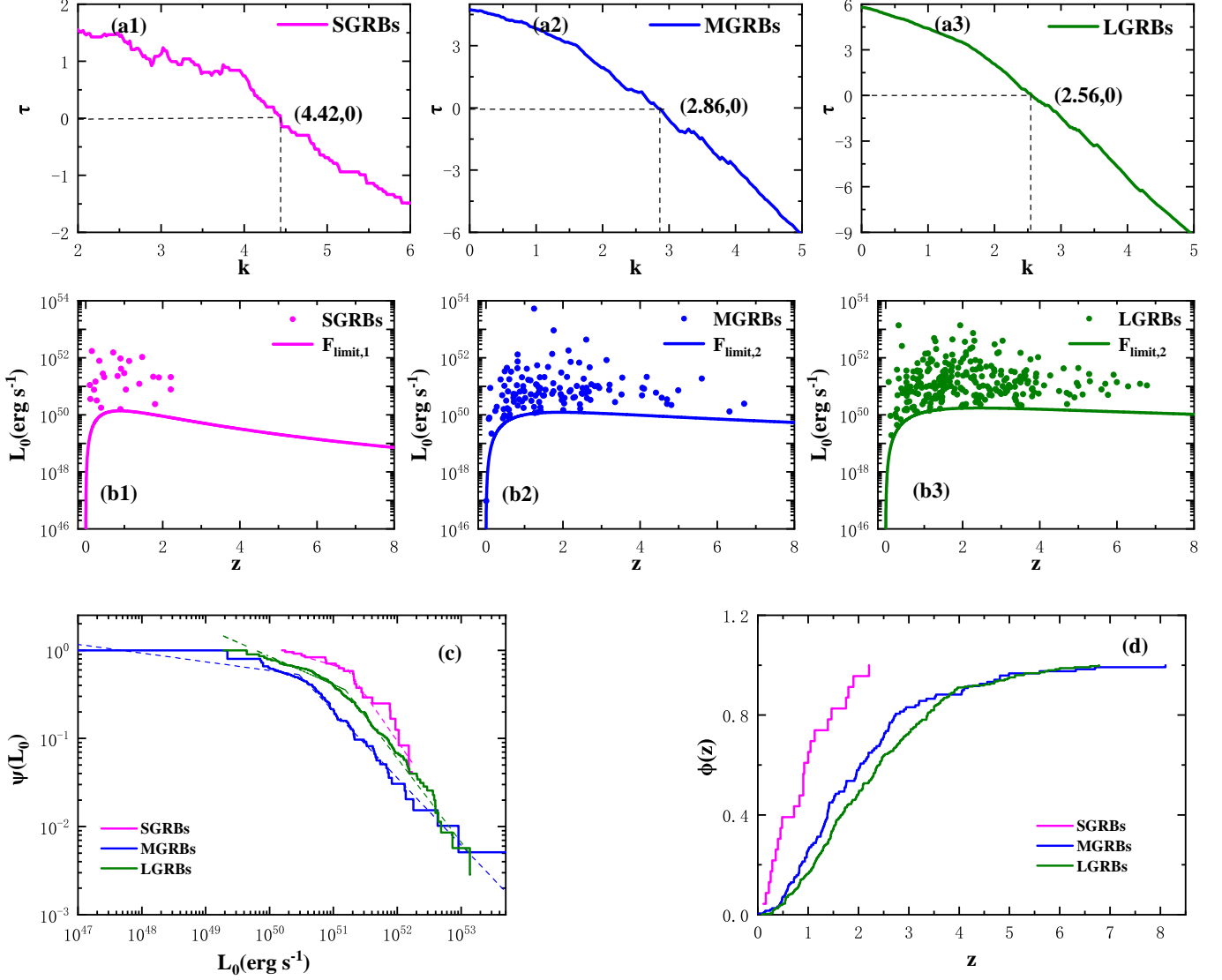


Figure 2. Different features of the three subclasses of GRBs. Panels (a1), (a2), and (a3) plot the test statistic τ versus k for SGRBs, MGRBs, and LGRBs, respectively. Panels (b1), (b2), and (b3) plot the de-evolved luminosity (L_0) versus the redshift (z) for the three samples. The solid lines represent the lower luminosity limits calculated from the two flux limits of $F_{\text{limit},1}$ and $F_{\text{limit},2}$, where $F_{\text{limit},1}$ is adopted for SGRBs, and $F_{\text{limit},2}$ is adopted for MGRBs and LGRBs. Panel (c) shows the cumulative luminosity function $\psi(L_0)$ of three samples, which is normalized to unity at the lowest luminosity. The dashed lines illustrate the best fit to the luminosity function by using a broken power-law function. Panel (d) shows the normalized cumulative redshift distribution of the three samples.

SGRBs, we get the best fit result as

$$\psi(L_0) \propto \begin{cases} L_0^{-0.22 \pm 0.01}, & L_0 \leq 1.68 \times 10^{51} \text{ erg}, \\ L_0^{-1.04 \pm 0.01}, & L_0 > 1.68 \times 10^{51} \text{ erg}. \end{cases} \quad (10)$$

For MGRBs, we have

$$\psi(L_0) \propto \begin{cases} L_0^{-0.10 \pm 0.01}, & L_0 \leq 2.89 \times 10^{50} \text{ erg}, \\ L_0^{-0.76 \pm 0.01}, & L_0 > 2.89 \times 10^{50} \text{ erg}. \end{cases} \quad (11)$$

For LGRBs, we have

$$\psi(L_0) \propto \begin{cases} L_0^{-0.32 \pm 0.01}, & L_0 \leq 1.52 \times 10^{51} \text{ erg}, \\ L_0^{-0.95 \pm 0.01}, & L_0 > 1.52 \times 10^{51} \text{ erg}. \end{cases} \quad (12)$$

We see that the best fit functions are different for the three groups, both in the characteristic breaking energy and the power-law indices.

Panel (d) of Figure 2 shows the cumulative redshift distribution $\phi(z)$ of SGRBs, MGRBs, and LGRBs, correspondingly. We see that $\phi(z)$ are different for the three subclasses. The formation rate ($\rho(z)$) of GRBs can be further calculated from $d\phi(z)/dz$ as

$$\rho(z) = \frac{d\phi(z)}{dz} (1+z) \left(\frac{dV(z)}{dz} \right)^{-1}, \quad (13)$$

where

$$\frac{dV(z)}{dz} = \frac{c}{H_0} \frac{4\pi d_L^2(z)}{(1+z)^2} \frac{1}{\sqrt{1-\Omega_m + \Omega_m(1+z)^3}}. \quad (14)$$

Figure 3 illustrates the GRB formation rate as a function of redshift, plotted for SGRBs, MGRBs, and LGRBs, respectively. For comparison, the observed SFR data taken from Hopkins (2004), Thompson et al. (2006), Mannucci et al. (2007), Ota et al. (2008), Bouwens et al. (2008), Bouwens et al. (2011) are also plotted. Generally, the formation rates of the three subclasses decrease monotonously as the redshift increases. They all clearly exceed the SFR at $z < 1$. Additionally, the formation rates are obviously different for the three groups. Especially, the $\rho(z)$ of SGRBs differs from that of the other two groups significantly. A simple power-law function has been adopted to fit the $\rho(z)$ of these three samples. The power-law indices are -3.58 ± 0.61 , -1.54 ± 0.19 , and -0.79 ± 0.12 for SGRBs, MGRBs, and LGRBs, respectively. The K-S test has been adopted to compare the formation rate of each pair of the three groups, which gives the P-values as $p_{12} = 6.1 \times 10^{-2}$, $p_{13} = 2.7 \times 10^{-3}$, and $p_{23} = 0.43$. It further supports that the three subgroups are distinct categories.

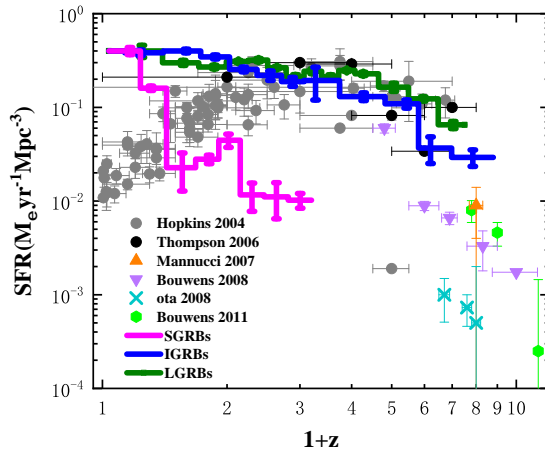


Figure 3. The formation rate of GRBs ($\rho(z)$) versus redshift for SGRBs (heavy pink stepped line), MGRBs (blue stepped line), and LGRBs (green stepped line). The rate is normalized to unity at the first data point. A simple power-law function is adopted to fit $\rho(z)$. The resultant slopes are -3.58 ± 0.61 , -1.54 ± 0.19 , and -0.79 ± 0.12 , for SGRBs, MGRBs, and LGRBs, respectively. For comparison, the observed SFR are also plotted, with the data taken from Hopkins (2004) (gray dots), Thompson et al. (2006) (black dots), Mannucci et al. (2007) (triangles), Ota et al. (2008) (crosses), Bouwens et al. (2008) (inverted triangles), Bouwens et al. (2011) (orange pentagons).

5. CONCLUSIONS

In this study, we investigate the long/short classification of *Swift*/*BAT* GRBs and the corresponding redshift distribution and event rate of each subclass. The intrinsic characteristic spectral hardness ratio is further included

as a useful supplement for the classification. The GMM models are used to fit the T_{90} distribution of GRBs, and both AIC and BIC criteria are adopted to assess the goodness of fit. It is found that the T_{90} distribution can be well fitted by the 3-G model, which means they can be grouped into three classes, i.e. short GRBs, intermediate GRBs, and long GRBs. Comparing with the results of Zhang et al. (2016), it is also found that the presence of intermediate class becomes more significant as the number of GRBs in the sample increases. When the spectral hardness ratio is included, the best fitting model is still 3-G. For GRBs with a known redshift so that the peak luminosity is available, we go further to study the redshift distribution and event rate of the three subclasses (SGRBs, MGRBs, and LGRBs) by using the EP-L method. It is found that the luminosity evolves with redshift as $L = L_0(1+z)^k$, with $k = 4.43, 2.86, 2.56$ for SGRBs, MGRBs and LGRBs, respectively. The results are consistent with previous studies in the cases of short GRBs (Zhang & Wang 2018; Dainotti et al. 2021b), and long GRBs (Yonetoku et al. 2004; Yu et al. 2015; Petrosian et al. 2015; Pescalli et al. 2016). Interestingly, for the three subclasses, significant difference exists in the cumulative luminosity function $\psi(L_0)$ as well as in the event rate $\rho(z)$, further supporting the existence of the intermediate subclass.

For the intermediate subclass GRBs, we notice that their T_{90} are mostly larger than 2s but less than 30s, and their spectra are relatively soft, which make them quite similar to classical long GRBs. However, the synthesized information from the redshift distribution and event rate indicates that they form a distinct subclass. Note that observational selection effect may still exist and could lead to some confusion in the classification of GRBs (Qin 2013). A significantly expanded sample size will help overcome this problem in the future. On the Other hand, the existence of the intermediate subclass of GRBs is not completely unexpected in theoretical aspect. In fact, it is not necessary that all long bursts with $T_{90} > 2s$ should uniquely originate from the collapse of massive stars. For example, it has been argued that some events may be due to the kick of high speed neutron stars (Huang et al. 2003; Xu et al. 2022). In addition, the existence of GRBs with extended emission component is another factor that challenges the traditional long/short GRB classification. It is expected that mechanisms other than traditional collapsars and binary compact star mergers may produce at least a small portion of GRBs.

ACKNOWLEDGEMENTS

1 We thank the anonymous referee for valuable suggestions that led to an overall improvement of this study. Our work
 2 was supported by the National Natural Science Foundation of China (Grant Nos. 12233002, 12373032, 12365011),
 3 by the National Key R&D Program of China (2021YFA0718500), and by the National SKA Program of China No.
 4 2020SKA0120300, by the Youth Science & Technology Talents Development Project of Guizhou Education Department
 5 (No. KY[2022]098), by the Project of Guizhou Vocational College of Economics and Business (No. Gzjm[2023]01).
 6 YFH also acknowledges the support from the Xinjiang Tianchi Program.

REFERENCES

- Akaike, H. 1974, IEEE Transactions on Automatic Control, 19, 716
- Bouwens, R. J., Illingworth, G. D., Franx, M., & Ford, H. 2008, ApJ, 686, 230, doi: [10.1086/590103](https://doi.org/10.1086/590103)
- Bouwens, R. J., Illingworth, G. D., Labbe, I., et al. 2011, Nature, 469, 504, doi: [10.1038/nature09717](https://doi.org/10.1038/nature09717)
- Burnham, K. P., & Anderson, D. R. 2004, Sociological Methods & Research, 33, 261, doi: [10.1177/0049124104268644](https://doi.org/10.1177/0049124104268644)
- Butler, N. R., Bloom, J. S., & Poznanski, D. 2010, ApJ, 711, 495, doi: [10.1088/0004-637X/711/1/495](https://doi.org/10.1088/0004-637X/711/1/495)
- Cao, X.-F., Yu, Y.-W., Cheng, K. S., & Zheng, X.-P. 2011, MNRAS, 416, 2174, doi: [10.1111/j.1365-2966.2011.19194.x](https://doi.org/10.1111/j.1365-2966.2011.19194.x)
- Dainotti, M., Levine, D., Fraija, N., & Chandra, P. 2021a, Galaxies, 9, 95, doi: [10.3390/galaxies9040095](https://doi.org/10.3390/galaxies9040095)
- Dainotti, M., Petrosian, V., Willingale, R., et al. 2015, MNRAS, 451, 3898, doi: [10.1093/mnras/stv1229](https://doi.org/10.1093/mnras/stv1229)
- Dainotti, M. G., Hernandez, X., Postnikov, S., et al. 2017a, ApJ, 848, 88, doi: [10.3847/1538-4357/aa8a6b](https://doi.org/10.3847/1538-4357/aa8a6b)
- Dainotti, M. G., Lenart, A. L., Sarracino, G., et al. 2020, ApJ, 904, 97, doi: [10.3847/1538-4357/abbe8a](https://doi.org/10.3847/1538-4357/abbe8a)
- Dainotti, M. G., Nagataki, S., Maeda, K., Postnikov, S., & Pian, E. 2017b, A&A, 600, A98, doi: [10.1051/0004-6361/201628384](https://doi.org/10.1051/0004-6361/201628384)
- Dainotti, M. G., Nielson, V., Sarracino, G., et al. 2022, MNRAS, 514, 1828, doi: [10.1093/mnras/stac1141](https://doi.org/10.1093/mnras/stac1141)
- Dainotti, M. G., Petrosian, V., & Bowden, L. 2021b, ApJL, 914, L40, doi: [10.3847/2041-8213/abf5e4](https://doi.org/10.3847/2041-8213/abf5e4)

- Dainotti, M. G., Petrosian, V., Singal, J., & Ostrowski, M. 2013, *ApJ*, 774, 157, doi: [10.1088/0004-637X/774/2/157](https://doi.org/10.1088/0004-637X/774/2/157)
- Deng, C.-M., Wang, X.-G., Guo, B.-B., et al. 2016, *ApJ*, 820, 66, doi: [10.3847/0004-637X/820/1/66](https://doi.org/10.3847/0004-637X/820/1/66)
- Dong, X. F., Li, X. J., Zhang, Z. B., & Zhang, X. L. 2022, *MNRAS*, 513, 1078, doi: [10.1093/mnras/stac949](https://doi.org/10.1093/mnras/stac949)
- Dörre, A., & Emura, T. 2019, *Nonparametric Inference for Double-Truncation* (Singapore: Springer Singapore), 63–74, doi: [10.1007/978-981-13-6241-5_4](https://doi.org/10.1007/978-981-13-6241-5_4)
- Efron, B., & Petrosian, V. 1992, *ApJ*, 399, 345, doi: [10.1086/171931](https://doi.org/10.1086/171931)
- Efron, B., & Petrosian, V. 1998, *Nonparametric Methods for Doubly Truncated Data*. <https://arxiv.org/abs/astro-ph/9808334>
- Efstathiou, G., Ellis, R. S., & Peterson, B. A. 1988, *MNRAS*, 232, 431, doi: [10.1093/mnras/232.2.431](https://doi.org/10.1093/mnras/232.2.431)
- Elliott, J., Greiner, J., Khochfar, S., et al. 2012, *A&A*, 539, A113, doi: [10.1051/0004-6361/201118561](https://doi.org/10.1051/0004-6361/201118561)
- Gehrels, N., Chincarini, G., Giommi, P., et al. 2004, *ApJ*, 611, 1005, doi: [10.1086/422091](https://doi.org/10.1086/422091)
- Hopkins, A. M. 2004, *ApJ*, 615, 209, doi: [10.1086/424032](https://doi.org/10.1086/424032)
- Horváth, I. 1998, *ApJ*, 508, 757, doi: [10.1086/306416](https://doi.org/10.1086/306416)
- . 2002, *A&A*, 392, 791, doi: [10.1051/0004-6361:20020808](https://doi.org/10.1051/0004-6361:20020808)
- Howell, E. J., Coward, D. M., Stratta, G., Gendre, B., & Zhou, H. 2014, *MNRAS*, 444, 15, doi: [10.1093/mnras/stu1403](https://doi.org/10.1093/mnras/stu1403)
- Huang, Y. F., Dai, Z. G., Lu, T., Cheng, K. S., & Wu, X. F. 2003, *ApJ*, 594, 919, doi: [10.1086/377129](https://doi.org/10.1086/377129)
- Kass, R. E., & Raftery, A. E. 1995, *Journal of the American Statistical Association*, 90, 773, doi: [10.1080/01621459.1995.10476572](https://doi.org/10.1080/01621459.1995.10476572)
- Klebesadel, R. W., Strong, I. B., & Olson, R. A. 1973, *ApJL*, 182, L85, doi: [10.1086/181225](https://doi.org/10.1086/181225)
- Kouveliotou, C., Meegan, C. A., Fishman, G. J., et al. 1993, *ApJL*, 413, L101, doi: [10.1086/186969](https://doi.org/10.1086/186969)
- Liang, E., Zhang, B., Virgili, F., & Dai, Z. G. 2007, *ApJ*, 662, 1111, doi: [10.1086/517959](https://doi.org/10.1086/517959)
- Liddle, A. R. 2007, *MNRAS*, 377, L74, doi: [10.1111/j.1745-3933.2007.00306.x](https://doi.org/10.1111/j.1745-3933.2007.00306.x)
- Lloyd, N. M., & Petrosian, V. 1999, *ApJ*, 511, 550, doi: [10.1086/306719](https://doi.org/10.1086/306719)
- Lynden-Bell, D. 1971, *MNRAS*, 155, 95, doi: [10.1093/mnras/155.1.95](https://doi.org/10.1093/mnras/155.1.95)
- Mannucci, F., Buttery, H., Maiolino, R., Marconi, A., & Pozzetti, L. 2007, *A&A*, 461, 423, doi: [10.1051/0004-6361:20065993](https://doi.org/10.1051/0004-6361:20065993)
- McBreen, B., Hurley, K. J., Long, R., & Metcalfe, L. 1994, *MNRAS*, 271, 662, doi: [10.1093/mnras/271.3.662](https://doi.org/10.1093/mnras/271.3.662)
- Ota, K., Iye, M., Kashikawa, N., et al. 2008, *ApJ*, 677, 12, doi: [10.1086/529006](https://doi.org/10.1086/529006)
- Paczynski, B. 1998, *ApJL*, 494, L45, doi: [10.1086/311148](https://doi.org/10.1086/311148)
- Pescalli, A., Ghirlanda, G., Salvaterra, R., et al. 2016, *A&A*, 587, A40, doi: [10.1051/0004-6361/201526760](https://doi.org/10.1051/0004-6361/201526760)
- Petrosian, V., & Dainotti, M. G. 2024, *ApJL*, 963, L12, doi: [10.3847/2041-8213/ad2763](https://doi.org/10.3847/2041-8213/ad2763)
- Petrosian, V., Kitanidis, E., & Kocevski, D. 2015, *ApJ*, 806, 44, doi: [10.1088/0004-637X/806/1/44](https://doi.org/10.1088/0004-637X/806/1/44)
- Qin, Y. 2013, *ApJ*, 763, 15, doi: [10.1088/0004-637X/763/1/15](https://doi.org/10.1088/0004-637X/763/1/15)
- Robertson, B. E., & Ellis, R. S. 2012, *ApJ*, 744, 95, doi: [10.1088/0004-637X/744/2/95](https://doi.org/10.1088/0004-637X/744/2/95)
- Salvaterra, R., Campana, S., Vergani, S. D., et al. 2012, *ApJ*, 749, 68, doi: [10.1088/0004-637X/749/1/68](https://doi.org/10.1088/0004-637X/749/1/68)
- Schwarz, G. 1978, *The Annals of Statistics*, 6, 461, doi: [10.1214/aos/1176344136](https://doi.org/10.1214/aos/1176344136)
- Tarnopolski, M. 2015, *A&A*, 581, A29, doi: [10.1051/0004-6361/201526415](https://doi.org/10.1051/0004-6361/201526415)
- . 2019, *ApJ*, 870, 105, doi: [10.3847/1538-4357/aaf1c5](https://doi.org/10.3847/1538-4357/aaf1c5)
- Thompson, R. I., Eisenstein, D., Fan, X., et al. 2006, *ApJ*, 647, 787, doi: [10.1086/505568](https://doi.org/10.1086/505568)
- Tsutsui, R., & Shigeyama, T. 2014, *PASJ*, 66, 42, doi: [10.1093/pasj/psu008](https://doi.org/10.1093/pasj/psu008)
- Tsvetkova, A., Frederiks, D., Golenetskii, S., et al. 2017, *ApJ*, 850, 161, doi: [10.3847/1538-4357/aa96af](https://doi.org/10.3847/1538-4357/aa96af)
- Wanderman, D., & Piran, T. 2010, *MNRAS*, 406, 1944, doi: [10.1111/j.1365-2966.2010.16787.x](https://doi.org/10.1111/j.1365-2966.2010.16787.x)
- Wang, F. Y. 2013, *A&A*, 556, A90, doi: [10.1051/0004-6361/201321623](https://doi.org/10.1051/0004-6361/201321623)
- Wang, M.-C., Jewell, N. P., & Tsai, W.-Y. 1986, *The Annals of Statistics*, 14, 1597, doi: [10.1214/aos/1176350180](https://doi.org/10.1214/aos/1176350180)
- Woodroffe, M. 1985, *The Annals of Statistics*, 13, 163, doi: [10.1214/aos/1176346584](https://doi.org/10.1214/aos/1176346584)
- Woosley, S. E. 1993, *ApJ*, 405, 273, doi: [10.1086/172359](https://doi.org/10.1086/172359)
- Woosley, S. E., & Bloom, J. S. 2006, *ARA&A*, 44, 507, doi: [10.1146/annurev.astro.43.072103.150558](https://doi.org/10.1146/annurev.astro.43.072103.150558)
- Xu, F., Geng, J.-J., Wang, X., Li, L., & Huang, Y.-F. 2022, *MNRAS*, 509, 4916, doi: [10.1093/mnras/stab3342](https://doi.org/10.1093/mnras/stab3342)
- Yonetoku, D., Murakami, T., Nakamura, T., et al. 2004, *ApJ*, 609, 935, doi: [10.1086/421285](https://doi.org/10.1086/421285)
- Yu, H., Wang, F. Y., Dai, Z. G., & Cheng, K. S. 2015, *ApJS*, 218, 13, doi: [10.1088/0067-0049/218/1/13](https://doi.org/10.1088/0067-0049/218/1/13)
- Zhang, G. Q., & Wang, F. Y. 2018, *ApJ*, 852, 1, doi: [10.3847/1538-4357/aa9ce5](https://doi.org/10.3847/1538-4357/aa9ce5)
- Zhang, L., Luo, J.-J., Huang, Y.-F., Gong, Y.-J., & Wu, S. 2022, *MNRAS*, 517, 5770, doi: [10.1093/mnras/stac3131](https://doi.org/10.1093/mnras/stac3131)
- Zhang, Z.-B., Yang, E.-B., Choi, C.-S., & Chang, H.-Y. 2016, *MNRAS*, 462, 3243, doi: [10.1093/mnras/stw1835](https://doi.org/10.1093/mnras/stw1835)
- Zhang, Z. B., Zhang, C. T., Zhao, Y. X., et al. 2018, *PASP*, 130, 054202, doi: [10.1088/1538-3873/aaa6af](https://doi.org/10.1088/1538-3873/aaa6af)

Zitouni, H., Guessoum, N., Azzam, W. J., & Mochkovitch,
R. 2015, *Ap&SS*, 357, 7, doi: [10.1007/s10509-015-2311-x](https://doi.org/10.1007/s10509-015-2311-x)